Multisource Classification of Color and Hyperspectral Images Using Color Attribute Profiles and Composite Decision Fusion

Guy Thoonen, *Student Member, IEEE*, Zahid Mahmood, *Student Member, IEEE*, Stijn Peeters, and Paul Scheunders, *Member, IEEE*

***Abstract*—In this work, we treat the problem of combined classification of a high spatial resolution color image and a lower spatial resolution hyperspectral image of the same scene. The problem is particularly challenging, since we aim for classification maps at the spatial resolution of the color image. Contextual information is obtained from the color image by introducing Color Attribute Profiles (CAPs). Instead of treating the 'R', 'G', and 'B' bands separately, the color image is transformed into CIE-Lab space. In this color space, attribute profiles are extracted from the 'L' band, which corresponds to the Luminance, while the 'a' and 'b' bands, which contain the color information, are kept intact, and the resulting images are transformed back into RGB space. The spectral information is obtained from the hyperspectral image. A Composite Decision Fusion (CDF) strategy is proposed, combining a state-of-the-art kernel-based decision fusion technique with the popular composite kernel classification approach. Experiments are conducted, using simulated data and a real multisource dataset containing airborne hyperspectral data and orthophotographic data from a suburban area in Belgium. These experiments show that our CAPs perform well with respect to other approaches for extracting attribute profiles from high resolution color images, and that the proposed CDF strategy produces meaningful results with respect to concatenation and the highlighted state-of-the-art approaches for combining multisource data.**

***Index Terms*—Color, image classification, morphological operations, multisensor systems, multiresolution techniques.**

I. Introduction

HYPERSPECTRAL data have proven to be very useful for adequate discrimination between detailed materials [1]. Unfortunately, the high spectral detail of hyperspectral images comes with the trade-off of a lower spatial resolution [2]. With the advent of unmanned aerial vehicles (UAV), images with extremely high spatial resolution have become available at a relatively low cost. Typically, however, while the spatial detail goes in the sub-meter or even sub-decimeter range, these UAV are often equipped with simple, lightweight sensors, such as RGB cameras [3]. As a result, the acquired images show very little spectral detail of the scene under study. Nevertheless, in order to achieve satisfactory classification results, sufficient spectral information is invaluable. A combined use of the different available sensors can improve classification performance substantially.

In this paper, we describe a framework for the treatment of multisource data and in particular a color image of high spatial resolution and a hyperspectral image of lower spatial resolution. The problem is particularly challenging, because we aim for classification maps at the spatial resolution of the color image. We will discuss two aspects: the contextual feature extraction from the color image and a decision fusion strategy for the combination of both sources.

With respect to the first aspect, we postulate that all relevant spatial, contextual information is contained in the color image. Several strategies have been proposed for extracting contextual information from high-resolution remote sensing images. These strategies include Markov random fields [4], Gabor filters [5] and morphological profiles (MPs) [6]. While morphological operators were originally developed for binary images, different approaches exist for the extension to grayscale images. However, the extension towards color images is not at all straightforward. Of course, while it is possible to process the morphological operators on each of the color components separately, this approach often leads to artefacts because the existing correlations between the different color components is entirely lost. This correlation can be preserved by looking at the colors simultaneously, namely as vectors, and order these color vectors in the color model. Numerous ordering approaches exist, forming a major topic of research in the mathematical morphology field [7]. For instance, it is possible to order the set of input color vectors according to a single color component, or according to multiple color components in a sequential fashion [8], [9]. Alternatively, the vectors can be partitioned into groups [10] or ranked according to a derived scalar metric [11]. Other approaches exist [12], [13]. For a more detailed overview, the reader is referred to [7].

Recently, the concept of MPs has been generalized to attribute profiles (APs) [14]. Additionally, in [15], the concept of APs is further extended to high-resolution hyperspectral images, by considering several of the principal components (PCs) of the image and generating an AP for each of these PCs. By combination of all the separate APs, an extended attribute profile (EAP) is constructed [16], [17].

In this paper, color attribute profiles (CAPs) are introduced, specifically for color remote sensing images. The aim of these

Manuscript received July 27, 2011; revised September 06, 2011; accepted September 06, 2011. Date of publication October 20, 2011; date of current version May 23, 2012. This work was supported by the Belgian Science Policy Office under the framework of the STEREO program project HABISTAT (contract SR/00/103).

The authors are with IBBT, Vision Lab, Department of Physics, University of Antwerp, 2610 Wilrijk, Belgium (corresponding author, e-mail: Guy.Thoonen@ua.ac.be).

Color versions of one or more of the figures in this paper are available online at http://ieeexplore.ieee.org.

Digital Object Identifier 10.1109/JSTARS.2011.2168317

CAPs is to take into account the contextual and the color information that is present in the image. Contrary to the approach of the EAP, however, the AP is not generated on the 'R', 'G', and 'B' bands separately. Instead, the three bands are processed simultaneously. To this end, the original RGB image is transformed into CIE-Lab color space. In this color space, an AP is generated for the 'L' (Luminance) component, while the 'a' and 'b' components, containing the color information, are kept unchanged. Finally, the processed 'L' component and original 'a' and 'b' components are rejoined and the image is transformed back into RGB space, resulting in a CAP.

Since the hyperspectral image contains most of the spectral information of the scene, a pixelwise spectral classification is preferable. The second aspect that we address is the way to combine the spatial information, obtained from the color image, with the spectral information, obtained from the hyperspectral image. The most straightforward technique of combination is a concatenation of the involved feature sets into one feature space and a classification of the resulting feature set [18]–[20]. In recent literature, other strategies for the combination of different sources of information, based on decision fusion were described. Most of these techniques rely on kernel-based classification techniques, because they are known for their superior performance in high-dimensional problems. In [21], the concept of composite kernels is introduced for hyperspectral image classification. Composite kernels are a weighted combination of kernels, e.g., a kernel for the classification of spectral information and one for spatial information, allowing to include explicit cross relations between the spectral and the spatial information. Recently, in [22] a generalization of the composite kernel approach, using multiple kernels is proposed, based on an automatic update of a linear combination of classifiers. In [23], two sources of information (SAR and optical) are combined by using a separate support vector machine (SVM) classifier on each of the sources, followed by a decision fusion step, in which a third classifier processes the original outcomes of both SVMs. In [24], the same strategy is applied for hypertemporal data.

In this work, we are interested in assessing the relative contribution of the spectral and spatial information source, respectively. Therefore, we apply the strategy of weighted composite kernels, in our case combining a kernel for the spatial and a kernel for the spectral information. However, rather than directly combining both feature sets using a weighted composite kernel SVM, the spatial and the spectral feature sets are first classified separately, after which the composite kernel approach is applied on the outcomes of these separate SVMs. This way, the strategy of [23], which reduces the original feature sets to two smaller, more comparable, sets, and the strategy of [21], which allows control over the contribution of either contextual or spectral information, are effectively combined. We refer to this approach as composite decision fusion (CDF).

To validate the proposed techniques, we perform experiments on synthetic multisource datasets, where an original hyperspectral image is downscaled to obtain a lower spatial resolution image. The RGB image is obtained from the original image by selecting a 'R', 'G', and 'B' band. We also perform an experiment on a real multisource dataset from a Belgian suburban area, containing a hyperspectral image of 2.5 m resolution and a high-spatial resolution (0.25 m) RGB image obtained from available orthophotographs. We show that the classification accuracy benefits from using our CAPs, compared to using a grayscale AP or even compared to other strategies for gathering APs in CIE-Lab color space, e.g., processing all three of the 'L', 'a' and 'b' components separately. We also show that the proposed CDF strategy outperforms concatenation and the decision fusion strategies of [21] and [23]. Moreover, the weight between both kernels can be applied as a trade-off between spectral and spatial accuracies of the obtained classification maps.

In Section II, the contextual feature extraction is discussed. We provide a brief review of APs and introduce the CAPs. In Section III, the decision fusion strategies are elaborated. Experiments and results are shown in Section IV. Finally, Section V summarizes and presents the conclusions of this work.

II. Contextual Feature Extraction

A. Attribute Profiles

In [6], a single morphological feature is generated by performing a morphological opening or closing by reconstruction on the original grayscale image. The MP consists of multiple of these morphological features, generated with a structuring element of increasing size. In [25], the MP concept is extended to high-resolution hyperspectral images, by considering several of the PCs of the image and generating a MP for each of these PCs separately. By combining all these MPs, an extended morphological profile (EMP) is constructed.

In [14], morphological attribute profiles (APs) are proposed as a more general approach to the extraction of contextual information from high resolution images than conventional MPs. Regular MPs depend strongly on the shape of a structural element and are mostly limited to the characterization of the scale of objects in the scene. APs, on the other hand, are not based on a predefined structural element. In addition, depending on the choice of the attributes, various types of structural information can be extracted. Possible attributes include Area, i.e., the size of the regions, Moment of Inertia, which models the elongation of the objects in the scene, and Standard Deviation, modeling region homogeneity. For instance, the Area opening attribute preserves or removes regions from the image, depending on whether, in this case, the area (hereafter referred to as the criterion) of these regions is larger or smaller than a predefined value (referred to as the threshold), respectively. An attribute opening profile is then generated by acquiring an opening attribute for multiple values of the threshold. Characterizing an image with several types of attributes leads to a more complete and accurate description of the spatial structures compared to conventional MPs.

In practice, the construction of APs is based on attribute filters, as introduced by Breen and Jones [26], which test a criterion, for instance an increasing criterion, on the connected components of the image. In the simple case of a binary image, a connected component is a set of pixels in which each pair of pixels is connected according to a connectivity rule, e.g., the four- and eight-connectivity, where a pixel is said to be adjacent

to four or eight of its neighboring pixels, respectively. A criterion T is increasing if the fact that region C satisfies T implies that region D satisfies T, given that $D \subseteq C$. If the increasing criterion is not met for a connected component, it is completely removed. Vice versa, if the criterion is met, the connected component is completely preserved.

More formally, the binary connected opening $\Gamma_x(X)$ of a binary image X extracts the connected component to which the pixel x belongs and removes all the other connected components. The binary trivial opening $\Gamma_T(C)$ of a connected component C with criterion T returns the component C if C satisfies T, while C is removed otherwise. Finally, the binary attribute opening $\Gamma^T(X)$ of X with criterion T is given by

$$\Gamma^T(X) = \bigcup_{x \in X} \Gamma_T[\Gamma_x(X)]. \quad (1)$$

From (1), it is clear that the attribute opening is equivalent to performing a trivial opening on all connected components in the image, i.e., removing all connected components that do not meet the criterion. All the definitions above can be extended to the respective dual transformations, to determine the binary attribute closing. Generally, if the criterion is non-increasing, we no longer speak of opening and closing, rather of thinning and thickening.

The extension from binary to grayscale attribute operators is possible by thresholding a grayscale image at each of its graylevels. This way, a stack of binary images is constructed. On each of these binary images, the binary attribute operators are applied. The grayscale attribute opening of a grayscale image I is then given by the maximum graylevel of the results of the filtering for each pixel,

$$\gamma^T(I)(x) = \max\{k | x \in \Gamma^T[Th_k(I)]\} \quad (2)$$

where $Th_k(I)$ is the binary image obtained by thresholding I at graylevel k. The grayscale attribute closing of a grayscale image is defined analogously. As a side note, in [14], the computational load for calculating the grayscale attribute is reduced drastically by an efficient data representation related to Max-Tree [27]. Although this data representation is not used in our experiments, our work does not introduce any constraints on its applicability and, consequently, the results presented in this article are expected to remain the same.

To conclude, the attribute opening profile $\Pi_{\gamma^T}(I)$ for a family of increasing criteria $T = \{T_\lambda, \lambda = 0, \ldots, n\}$, where T_λ is the criterion with threshold value λ, is defined as

$$\Pi_{\gamma^T}(I) = \{\Pi_{\gamma^{T_\lambda}} | \Pi_{\gamma^{T_\lambda}} = \gamma^{T_\lambda}(I), \forall \lambda \in [0, \ldots, n]\}. \quad (3)$$

Once again, the attribute closing profile is defined analogously. For further details, the reader is referred to [14].

B. Color Attribute Profiles

Similar to grayscale MPs, the extension of grayscale APs to multichannel images is not straightforward, because there is no unambiguous means of defining the minimum and maximum values between two vectors of more than one dimension. A simple way to extend the APs to multichannel data consists in applying the approach for grayscale images on each channel separately, a strategy referred to in literature as the marginal approach [28]. However, in marginal processing, the correlation among different channels, along with all extra information that could be used in order to improve the quality of the result, is completely ignored.

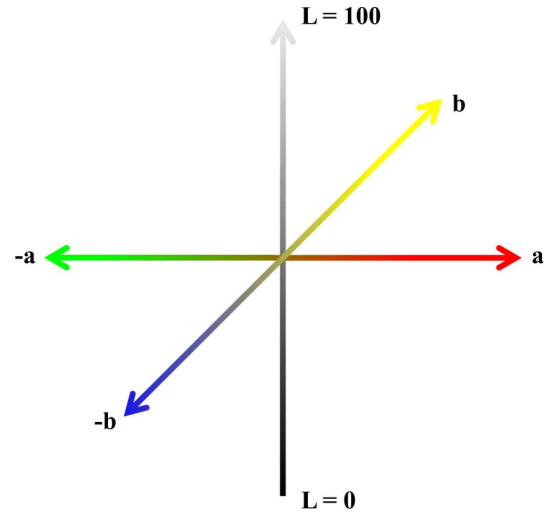

Fig. 1. Diagram representing the CIE-Lab color space.

A possible solution to this problem consists in applying a decorrelation transformation prior to using marginal processing for calculating the APs [29]. Principal component analysis (PCA) is implemented in [15] as a decorrelation transformation for hyperspectral images, followed by a marginal calculation of APs on the first PCs, which results in an EAP. However, when applying data dependent transformations, such as PCA, on color images, data differences are generally not highly correlated with perceptual color differences [30]. Alternatively, for color images, more specific color space transformations exist to perform decorrelation of the 'R', 'G', and 'B' bands, for instance the transformation to CIE-Lab color space.

CIE-Lab color space, just like other color spaces defined by the Commission Internationale de l'Eclairage (CIE), is based on the XYZ color space. Contrary to RGB space, every perceivable color can be uniquely constructed as an additive combination of the supersaturated standard color coordinates 'X', 'Y', and 'Z', that are derived from 'R', 'G', and 'B' bands by a linear transformation [31]. However, 'X', 'Y', and 'Z' do not correspond to real colors by themselves and, therefore, are difficult to use. Moreover, like in RGB space, XYZ space is not perceptually uniform, meaning that colors that are perceptually the same, are not necessarily close to each other in the color space. Therefore, CIE-Lab color space has been introduced by nonlinear transformation of the XYZ space, hereby constructing a color space with more intuitive components and geometrical distances that approximately show a uniform correspondence to perceptual distances. As illustrated in Fig. 1, the 'L' component represents the luminance and ranges from 0 (completely black) to 100 (completely white), the 'a' component represents the opponent colors red (positive) and green (negative), and the 'b' component represents the opponent colors yellow (positive) and blue (negative). For more details on the CIE-Lab system, the reader is referred to [32].

Since CIE-Lab color space is perceptually uniform, colors that appear to be similar to a human observer are very close together. Moreover, the human perception of luminance is highly correlated to the 'L' component in this color space [33]. Consequently, working in CIE-Lab color space, the 'L' component, which holds the luminance (intensity), is the most suitable for extracting APs, because it largely contains the contour information of the objects in the image [34]. The hue information is contained in the 'a' and 'b' components and can be used for the distinction between objects of a specific color. Consequently, in this work, the luminance component 'L' has been used to calculate the APs, while, to avoid the loss of color information, the 'a' and 'b' components are unprocessed. Recombining the 'L' APs with the original 'a' and 'b' components and transforming the image back into RGB color space results in color attribute profiles (CAPs).

The advantage of this approach is that the correlation between the three bands of each color attribute is almost the same as for the input color image. Besides the superior performance of the APs for extracting contextual information from the luminance image, the original color information of the remaining objects is preserved and, as a result, regions with similar luminance but distinct color information can still be distinguished.

In the experimental section, our proposed method is compared to other strategies for extracting APs from a color image, e.g., APs on only the luminance, discarding the 'a' and 'b' components, and APs by marginal processing of the 'L', 'a' and 'b' components.

III. Decision Fusion

A. Support Vector Machines

Since SVMs were applied extensively in remote sensing and, particularly, in hyperspectral image classification literature, we will limit ourselves to a very general description of SVMs and refer the reader to the literature. An overview of the use of SVMs in the remote sensing domain can, e.g., be found in [35] and [36].

SVMs fit a hyperplane to the training samples of two classes in the feature space by maximizing the margins between the hyperplane and the samples closest to it. Given a set of training samples $\{(\mathbf{x}_1, y_1), (\mathbf{x}_2, y_2), \ldots, (\mathbf{x}_n, y_n)\}$, where $\mathbf{x}_i \in \mathbb{R}^n$ is a single data instance and $y_i \in \{-1, 1\}$ is the corresponding label, the optimal hyperplane is described by the solution of

$$\min_{\mathbf{w},b,\xi_i} \frac{1}{2}\mathbf{w}^T\mathbf{w} + C\sum_i \xi_i \tag{4}$$

with additional constraints

$$y_i(\mathbf{w}^T\mathbf{x}_i + b) \geq 1 - \xi_i, \tag{5}$$

$$\xi_i \geq 0. \tag{6}$$

Here, $\mathbf{w}$ and b are the weight vector and the bias that describe the hyperplane, respectively. The slack variables, ξ_i, are introduced to satisfy the constraints for data that can not be totally separated linearly. In addition, the cost function C is a parameter set by the user to control the penalty assigned to errors.

Because most cases are not linearly separable, the input data are transformed to a higher-dimensional Hilbert space $\mathcal{H}$ by a nonlinear mapping function $\mathbf{\Phi} : \mathbb{R}^n \rightarrow \mathcal{H}$, allowing to apply a fitting of a linear hyperplane. However, by solving (4) using the Lagrangian dual formulation [35], all the mappings appear as inner products. Consequently, by defining a kernel function

$$K(\mathbf{x}_i, \mathbf{x}_j) = \langle \mathbf{\Phi}(\mathbf{x}_i), \mathbf{\Phi}(\mathbf{x}_j) \rangle \tag{7}$$

the mapping does not need to be performed explicitly. One of the most popular kernel functions, that has been shown to perform well [37], is the Radial Basis Function (RBF) kernel, defined as

$$K_{\text{RBF}}(\mathbf{x}_i, \mathbf{x}_j) = \exp\left(-\gamma \|\mathbf{x}_i - \mathbf{x}_j\|^2\right), \quad \gamma > 0. \tag{8}$$

The kernel parameter γ is to be set by the user. This parameter is estimated during the training phase, together with the penalty parameter C. Both are commonly found by performing cross-validation for a grid of predefined values for γ and C.

SVMs have originally been developed for binary classification problems. In general, the multiclass problem is split into binary problems using a one-against-one strategy or a one-against-all strategy. The first is shown to outperform the latter, since it results in a larger number of simpler hyperplanes contrary to a smaller number of more complex hyperplanes. In the one-against-one strategy, individual binary SVMs are trained for each pairwise classification problem. The primary output images contain the distances of each pixel to the hyperplane of the binary classification problem, and are referred to as rule images [23]. Likewise, for every pixel, a winning class label is associated with each of the binary SVMs. The final class membership of each pixel can be obtained by majority voting on the winning class labels.

B. Multisource Classification and Decision Fusion Strategies

With the availability of different sources of information, classification accuracies can be dramatically improved when classifiers account for all the information. To this purpose, the various sources of information need to be combined. In remote sensing, these information sources include e.g., feature sets obtained from multiple sensors (multispectral, hyperspectral, SAR, etc.) or multiple sets obtained from a single sensor (spatial/contextual features and spectral features). In our case, a high-spatial resolution RGB sensor and a hyperspectral sensor are in play. Moreover, the features obtained from the RGB image have a spatial/contextual nature while the features obtained from the hyperspectral image are purely spectral.

The most straightforward approach is a simple concatenation of the feature sets, in which the resulting set is fed into a single classifier. More practical combinations, however, are based on a separate classification for each of the feature sets and combine the obtained results using decision fusion strategies.

1) Composite Kernel: One particular class of techniques is the use of separate SVM kernels for each feature set. The combination of these kernels, the so-called composite kernel approach, is usually a weighted sum of the separate kernels. E.g., for two kernels K_a and K_b, the weighted composite kernel K_{a+b} is

$$K_{a+b}(\mathbf{x}_i, \mathbf{x}_j) = \beta K_a\left(\mathbf{x}_i^a, \mathbf{x}_j^a\right) + (1-\beta)K_b\left(\mathbf{x}_i^b, \mathbf{x}_j^b\right) \tag{9}$$

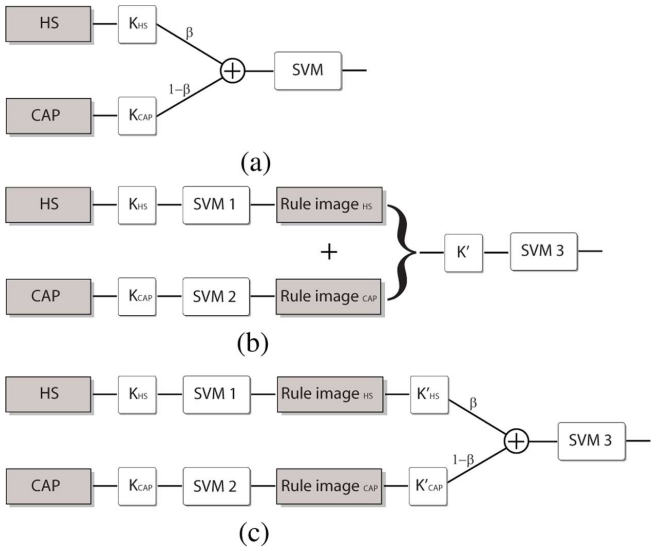

Fig. 2. Three strategies for combined classification of multisource data, consisting of hyperspectral (HS) data and contextual features in the form of CAPs. (a) Composite kernel approach. (b) SVM decision fusion approach. (c) Composite decision fusion approach.

Fig. 3. ROSIS data and area opening attribute image. (a) University area. (b) Color area opening ($\lambda = 1369$).

with β the weighting factor. This approach is illustrated in Fig. 2(a) for two feature sets, containing hyperspectral data and CAPs, which are extracted from the high-resolution color image. The advantage of such a composite kernel is a balancing of the spatial and spectral feature sets [21]. Recently, the concept of multiple kernels is introduced [22], where several kernels for each feature can be defined. The weights between the kernels are updated along with the kernel parameters during the training phase.

2) SVM Decision Fusion: Another branch of techniques involves separate classification of each of the feature sets and combination of the results using a specific decision fusion rule. Simple rules, such as majority voting, are applied. In [23], all rule images obtained from classifying different feature sets using SVMs, are stacked and fed as input to another classifier (e.g., a SVM) in a subsequent stage. The advantage of this technique is that distinct feature sets with different numbers of features and ranges of feature values are classified separately. The outputs of these classifiers are the rule images that contain, for each pixel, the distances to the hyperplanes between each pair of classes. Besides a dramatic data reduction, when applied as input to a new classifier, the number of features from each original subset is equal. Also, the values of the rule images are more comparable than the original feature sets, since each binary rule image is more appropriate to describe the interclass differences. These arguments were experimentally validated [23], [24]. The SVM Decision Fusion strategy is schematically depicted in Fig. 2(b) for the two feature sets that are involved in this work.

3) Composite Decision Fusion (CDF): In this work, we combine the concepts of composite/multiple kernels with the SVM decision fusion based on separate classifiers, as illustrated in Fig. 2(c) for the two data sets that are considered in this article. The advantages of both approaches can be combined. More in particular, we want to assess the relative contribution of the spatial/spectral information. This can be achieved by treating both data sets separately first, and then combining the obtained rule images using a composite kernel, using two separate kernels for the spatial/spectral data set and estimating the weight that determines the relative contribution of both sets, along with the kernel parameters. Moreover, the weight can be used as a parameter that balances between the relative contributions of the spectral resp. spatial image source. Note that the SVM decision fusion technique can be regarded as a special case of the CDF approach with equal kernels and weight $\beta = 0.5$.

IV. Experiments and Results

A. Experimental Setup

Two sets of experiments have been performed. The first set on simulated multisource data and the second set on real multisource data, consisting of a hyperspectral image and a high resolution orthophotographic color image.

1) Simulated Multisource Data: In the first set of experiments, hyperspectral data from the Reflective Optics System Imaging Spectrometer (ROSIS-3) are used, as shown in Fig. 3(a). The number of bands of the ROSIS-3 sensor is 115 with a spectral range from 430 nm to 860 nm. The training and validation sets are collected in the area around the University of Pavia, Italy, and consist of nine classes: Trees, asphalt, bitumen, gravel, metal sheets, shadow, self-blocking bricks, meadows and bare soil. The training set consists of approximately 4000 pixels, while the validation set consists of approximately 43,000 pixels. In addition to the training set, a disjoint test set of approximately 5000 pixels has been created, intended to tune the parameters during the training phase. Each band of the image has 610 rows and 310 columns. Twelve noisy bands have been removed, and the remaining 103 spectral channels are used for classification. A truecolor RGB image is extracted

Fig. 4. Orthophotographic data, AHS data and area opening attribute image of Kalmthout, (a) AHS image. (b) Orthophotographic image. (c) Color area opening ($\lambda = 1369$).

from the hyperspectral image, by selecting the three bands that correspond to the wavelengths closest to the center of the red, green, and blue spectral range, respectively. To simulate the situation where we have a high spatial resolution color image and a lower spatial resolution hyperspectral image, the hyperspectral image is downscaled by factor of 10 using a Gaussian filter. Subsequently, to combine the hyperspectral features with the contextual features extracted from the high resolution RGB image, the hyperspectral image is upscaled again by a factor of 10, using cubic convolution. The factor 10 resolution difference is selected as it is also the resolution difference between the two sets of the real multisource data. All experiments have also been performed for other resolution differences (factor 2 and factor 5) and show similar results.

2) Real Multisource Data: In the second series of experiments, real multisource imagery, including airborne hyperspectral data and orthophotographic data from a suburban area in Kalmthout, Belgium, are applied. The hyperspectral data originates from a flight campaign in June 2007 with an Airborne Hyperspectral Scanner (AHS) sensor with a ground resolution of approximately 2.5 m and is shown in Fig. 4(a). The range of 450–2550 nm is covered by 63 spectral bands. The orthophotographic data, depicted in Fig. 4(b), is a 3832×3833 pixels RGB color image of the same area that is part of a collection of images acquired in March and April 2007. The spatial resolution of this color image is approximately 0.25 m. Both data sets were georeferenced with information collected as image metadata during acquisition. To this end, a differential Global Positioning System (dGPS) and an Inertial Measurement Unit (IMU), providing orientation information, were used at the time of flight. Ground reference plots are manually delineated using the orthophotographic image, leading to over 1 million reference pixels. These reference pixels are subdivided into six classes: roofs, fields, flat roofs, bare soil, trees, and roads. Areas that are in visual disagreement between orthophotographic and hyperspectral data (for instance, some fields in the orthophotographic image appear as bare soil in the hyperspectral image due to the difference in acquisition time) are excluded from the set. Two disjoint subsets of approximately 6000 pixels are randomly selected from the complete set of ground reference data and serve the purpose of training and testing data, respectively. The remaining pixels are used as validation data. Fig. 5 illustrates the ground reference plots that have been delineated on the orthophotographic image. In order to combine the orthophotographic image with the hyperspectral data, the hyperspectral image has been resampled at the spatial resolution of the orthophotographic image, using cubic convolution.

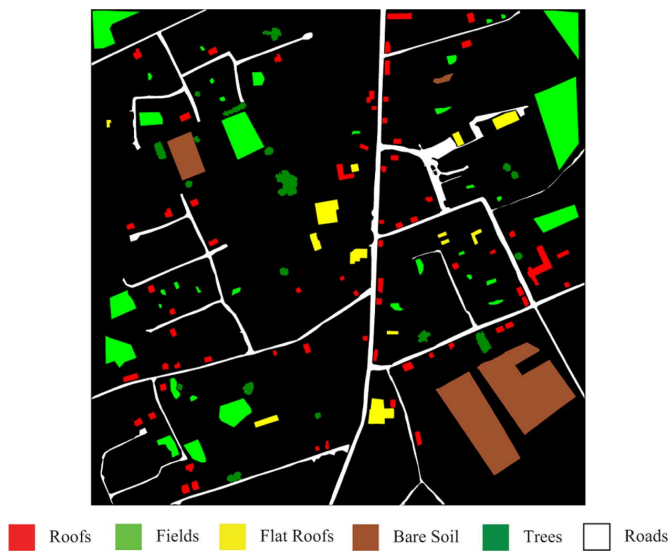

Fig. 5. Reference data of the Kalmthout area.

For both data sets, CAPs are calculated using Matlab and all SVM classifiers are implemented with RBF kernels using LIBSVM [38]. In the final step of both the Composite Kernel and the CDF approach, parameter selection is performed for each value of the weight β ranging from 0 to 1 in steps of 0.05, where $\beta = 0$ means pure spectral classification and $\beta = 1$ implies pure contextual classification. For each weight, two optimal RBF kernel parameters γ_1 and γ_2 are determined together with the penalty parameter C using a grid search. This way, a full set of parameters is available for a whole range of weights,

TABLE I
CLASSIFICATION ACCURACIES ON THE VALIDATION SET OF THE PAVIA UNIVERSITY DATA FOR THE COMPARISON OF CAP VERSUS OTHER STRATEGIES FOR EXTRACTING CONTEXTUAL INFORMATION. ALL COMBINATIONS OF CONTEXTUAL INFORMATION WITH HYPERSPECTRAL DATA ARE CLASSIFIED BY MEANS OF SIMPLE FEATURE CONCATENATION

Algorithm	Overall Accuracy OA	Kappa Coefficient κ	Average Accuracy
Hyperspectral only	77.48%	0.7109	73.46%
Hyperspectral + CAP	**85.91%**	**0.8172**	**84.11%**
CAP only	77.93%	0.7194	80.41%
Hyperspectral + Marginal AP	84.87%	0.8037	83.06%
Marginal AP only	76.02%	0.6989	80.86%
Hyperspectral + Gray AP	77.88%	0.7153	81.13%
Gray AP only	66.40%	0.5823	75.69%
Hyperspectral + L AP	81.59%	0.7629	79.14%
L AP only	68.23%	0.6038	73.58%

along with the overall accuracies on the separate test set. However, due to the size of the data, full classification is not performed on the validation set or on the full image for the complete range of β values. Instead, only a few values for β are selected for this purpose.

It is worth to notice that, performing a grid search to optimize two kernel parameters and one penalty parameter for 20 values of the weight value β, is a computationally very intensive operation. Running this grid search for one single value of β, takes approximately 1.5 hours on eight processor cores using Matlab's Parallel Processing Toolbox. Since the processing time does not depend on the value of β, the complexity scales linearly with the number of β values. However, the complexity of the CDF algorithm is not necessarily higher than the complexity of a direct Composite kernel classification, because the first stage of CDF performs a considerable feature reduction, somewhat reducing the complexity of the subsequent series of grid searches. Also, while it is not the aim of this paper, processing time can be considerably reduced by investigating other parameter selection strategies [39].

To construct the CAPs, three different attributes are used: 1) area; 2) moment of inertia, and 3) standard deviation. Following values of λ are used to find the Area attribute: 49, 169, 361, 625, 961, 1369, 1849, and 2401, similar to the thresholds selected in [14]. For the Moment of Inertia, following thresholds are applied: 0.2, 0.3, 0.4, 0.5, 0.6, 0.7, 0.8, and 0.9, also similar to [14]. The Standard Deviation attribute is built with the following threshold values: 5, 10, and 15, once again adopting the values selected in [14], but omitting the values of the thresholds which generated nearly empty features. The same attributes are chosen for the other APs in the comparison. Fig. 3(b) illustrates the result of a color area opening on the ROSIS image with a threshold $\lambda = 1369$. Fig. 4(c) shows the same on the orthophotographic data from Kalmthout. These examples already provide a good qualitative idea about the color preservation capabilities of the CAP. In the following subsection, experiments showing quantitative results are performed.

B. Experiments on the Simulated Image

1) CAPs Versus Other Strategies for Extracting Contextual Information: The first experiment on the simulated data compares the classification performance of the proposed CAPs to other approaches for extracting APs from an RGB color image. These include:

- Grayscale APs, using a grayscale image, obtained by direct conversion of the RGB image to YUV color space and removal of the chrominance information (U and V) [31] (Gray AP);
- APs calculated on the 'L' component only, without recombining with 'a' and 'b' (L AP);
- APs calculated by marginal processing of 'L', 'a' and 'b' components, transformed back into RGB space (Marginal AP).

In this experiment, all APs are classified both separately and together with the hyperspectral data, using simple feature concatenation only.

Table I shows the overall accuracies on the validation set for this classification experiment. From this table, it is clear that the CAP, combined with the hyperspectral data, yields the highest overall accuracy (OA), the highest kappa coefficient and the highest average class accuracy. In addition to the contours present in the CAP, the preserved colors clearly add a great deal of information. This can be seen very well when comparing with the accuracies of 'Gray AP' and 'L AP'. Not only do these results produce relatively low accuracies when classifying without merging with the hyperspectral features, but the accuracies also do not end up as high after concatenation. Although the methodology to produce the Marginal AP is the most similar to the construction of the CAP, the obtained accuracy is not as good. Like the construction of the CAP, structural information is extracted from the 'L' component and the 'a' and 'b' components are not discarded. However, for the Marginal AP, APs are constructed for the latter two components. This result demonstrates that preserving the color information is more beneficial than trying to extract contextual information from it. For this reason, the CAP is selected as the extraction method of choice for contextual information in the following experiments. Additionally, although a very simple feature fusion approach is applied in this experiment, the other fusion strategies show similar relative performances between the feature sets.

2) CDF Approach Versus Other Approaches for Combining Spectral and Contextual Information: The proposed CDF technique is compared to other combinations of the contextual and the spectral feature sets: a simple concatenation of all features into one SVM (Hyperspectral + CAP), a direct weighted Composite Kernel (Composite) and the SVM Decision Fusion technique (Decision Fusion). In addition, the classification of the CAP without merging with the hyperspectral image is once

TABLE II
CLASSIFICATION ACCURACIES ON THE VALIDATION SET OF THE PAVIA UNIVERSITY DATA FOR THE COMPARISON OF THE PROPOSED CDF APPROACH VERSUS OTHER APPROACHES FOR COMBINING SPECTRAL AND CONTEXTUAL INFORMATION

Algorithm	Overall Accuracy OA	Kappa Coefficient κ	Average Accuracy
Hyperspectral only	77.48%	0.7109	73.46%
CAP only	77.93%	0.7194	80.41%
Hyperspectral + CAP	85.91%	0.8172	84.11%
Decision Fusion	92.82%	0.9048	90.48%
Composite ($\beta = 0.65$)	86.86%	0.8271	85.10%
CDF ($\beta = 0.25$)	**93.87%**	**0.9192**	**91.81%**

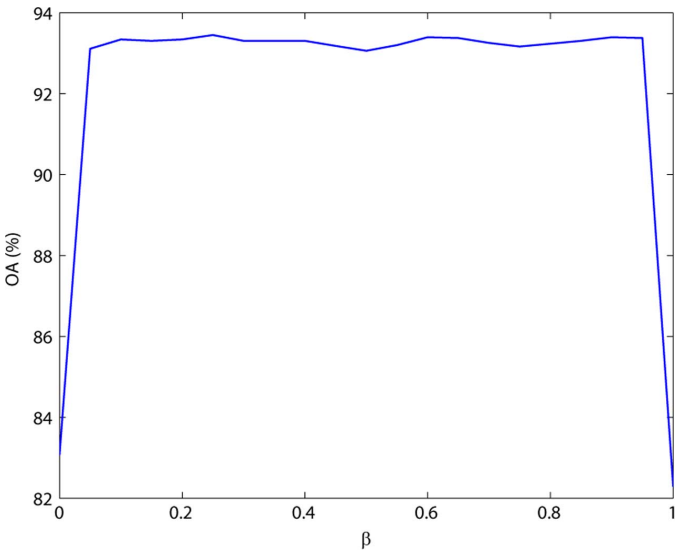

Fig. 6. Overall accuracies on the test set of the Pavia University data for the CDF approach in function of the kernel weight β.

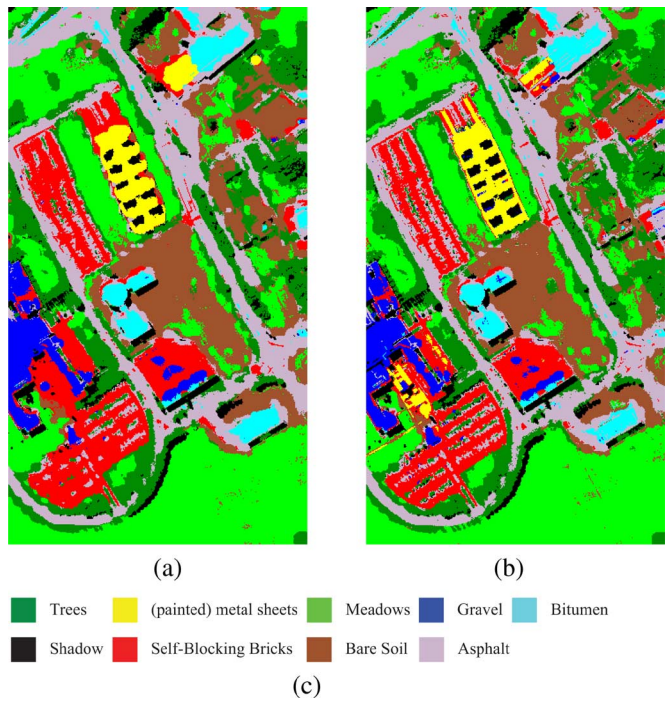

Fig. 7. Influence of the weight parameter on thematic maps of the Pavia University data obtained with the composite fusion strategy. (a) $\beta = 0.05$. (b) $\beta = 0.95$. (c) Legend.

again added for comparison (CAP only), as well as the classification of the hyperspectral data only (Hyperspectral only). In the following results, only the accuracies for the obtained optimal weights β are provided. Table II depicts the accuracies on the validation set for this classification experiment.

Evaluating these results, it is clear that all methods to combine both data sources outperform the simple concatenation approach. Moreover, the extra data reduction step leads to a significant improvement in accuracy. The CDF approach shows the highest OA. While the result of the decision fusion technique of [23] is very good as well, CDF is expected to perform at least as good as this technique, as explained in Section III.B.3. In the remaining experiments, CDF is selected as the strategy of choice for combining hyperspectral data and CAP.

3) CDF Approach for Various Values of the Kernel Weight: In the third experiment, the influence of the weight parameter of the CDF approach is investigated. Fig. 6 shows the overall accuracies obtained by varying the weight. For complexity reasons, these accuracies are obtained on the separate test set, as explained in Section IV-A. The figure shows a fairly flat response with respect to the variation of the weight parameter, save for the extreme values. Between the weight of 0.05 and 0.95, the variation in accuracy is less than 0.4%. Clearly, both kernel parameters γ_1 and γ_2, as well as the penalty parameter C compensate for the change in weight. This result encourages us to inspect the effect of the varying weight on the classification of the validation set and of the full image.

Two edge values are selected for the weight parameter to monitor the effect on the validation accuracy and on the appearance of the classified image. The β values selected are 0.05 (i.e., a very large weight on the spectral set) and 0.95 (i.e., a very large weight on the contextual set). Even on the validation set, the effect of the weight parameter appears to be rather small, yielding accuracies of 93.57% and 93.74% for $\beta = 0.05$ and $\beta = 0.95$, respectively. However, when considering the corresponding thematic maps, depicted in Fig. 7, the effect of the weight is in fact very large. The result for $\beta = 0.95$ shows finer delineations of the borders between classes and, consequently, object shapes are much more clear. This result is confirmed by the McNemar statistic for comparing two classification results [40], yielding a value of 2.11 in favor of the result with $\beta = 0.95$. This value corresponds to a significant difference, with a confidence larger than 95%.

To conclude, the test set is clearly representable for the validation set and the composite kernel parameter selection shows a

TABLE III
CLASSIFICATION ACCURACIES OF THE KALMTHOUT DATA FOR THE COMPARISON OF CAP VERSUS OTHER STRATEGIES FOR EXTRACTING CONTEXTUAL INFORMATION. ALL COMBINATIONS OF CONTEXTUAL INFORMATION WITH HYPERSPECTRAL DATA ARE CLASSIFIED BY MEANS OF SIMPLE FEATURE CONCATENATION

Algorithm	Overall Accuracy OA	Kappa Coefficient κ	Average Accuracy
Hyperspectral only	77.57%	0.7021	61.45%
Hyperspectral + CAP	**87.92%**	**0.8406**	**76.85%**
CAP only	85.35%	0.8070	74.87%
Hyperspectral + Marginal AP	87.51%	0.8352	76.03%
Marginal AP only	85.01%	0.8028	74.13%
Hyperspectral + Gray AP	84.00%	0.7886	70.32%
Gray AP only	73.16%	0.6455	59.22%
Hyperspectral + L AP	83.35%	0.7799	69.12%
L AP only	73.87%	0.6557	60.60%

TABLE IV
CLASSIFICATION ACCURACIES OF THE KALMTHOUT DATA FOR THE COMPARISON OF THE PROPOSED COMPOSITE DECISION FUSION APPROACH VERSUS OTHER APPROACHES FOR COMBINING SPECTRAL AND CONTEXTUAL INFORMATION

Algorithm	Overall Accuracy OA	Kappa Coefficient κ	Average Accuracy
Hyperspectral only	77.57%	0.7021	61.45%
CAP only	85.35%	0.8070	74.87%
Hyperspectral + CAP	87.92%	0.8406	76.85%
Decision Fusion	90.69%	0.8768	79.88%
Composite ($\beta = 0.65$)	89.78%	0.8657	**81.26%**
CDF ($\beta = 0.50$)	**90.71%**	**0.8770**	79.99%

compensating behavior for the effect of the kernel weight on the accuracies. However, the reference data contain very little information on transition areas between classes, a situation which often occurs in practice, due to the high cost and time consumption of ground reference collection [41]. Consequently, the weight parameter still offers the user the freedom to perform a qualitative tweaking towards smoother or finer edges.

C. Experiments on the Real Multisource Data Set

All the experiments that have been performed on the simulated multisource data have been verified on the real multisource data set and yield similar results and conclusions:

- The CAP outperforms the other strategies for extracting contextual information that are considered in this work, as illustrated in Table III. Once again, for this experiment, all multisource classification results have been generated by simple concatenation of the two feature sets. These results confirm the results from Table I.
- CDF yields the highest OA and Kappa coefficient with respect to simple concatenation and the other strategies for combined classification of multiple data sets that we have looked at, although the difference with the decision fusion strategy is small, as illustrated in Table IV. The average class accuracy of the direct Composite kernel approach is higher than the average accuracy of CDF, indicating that some of the smaller classes yield higher accuracies in the Composite approach.
- Fig. 8 shows the overall accuracies on the test set obtained by varying the weight. As expected, the accuracy shows a very flat response in function of the weight, except for the extreme values. This result is in agreement with the result for the simulated multisource data. The overall accuracy on the test set versus the weight is very flat, with a variation in accuracy of approximately 0.1%, but the weight allows a certain level of control over the crispness of the resulting thematic maps.

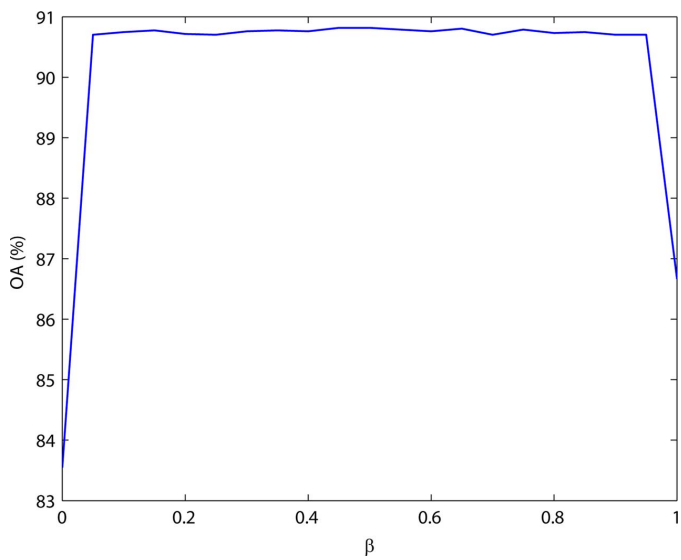

Fig. 8. Overall accuracies on the test set of the Kalmthout data for the composite fusion approach in function of the kernel weight β.

This section shows a more detailed study of the effect of using CDF to combine hyperspectral data and CAP with respect to separate classification of either hyperspectral data or CAP and to their combination by simple feature merging. Fig. 9 shows the effect of these strategies on the resulting thematic maps. In addition, the OA of the various strategies are shown. The hyperspectral only result, in Fig. 9(a), shows a reasonably homogeneous map, but a lot of the road structures and finer delineations are missing. Fig. 9(b) shows the CAP only result. This result

Fig. 9. The effect of combining hyperspectral data and CAP by simple concatenation and CDF on the classification result of the Kalmthout data, (a) Hyperspectral only (OA 77.57%). (b) CAP only (OA 85.35%). (c) Hyperspectral + CAP (OA 87.92%). (d) CDF ($\beta = 0.50$) (OA 90.71%).

shows much more structure than the pure hyperspectral map. However, there is a lot of confusion, for instance between the 'Roof' and the 'Tree' class. In addition, there is a lot of overlap between the 'Roof' and the 'Road' class. Concatenating hyperspectral data and CAP shows finer structures that are labelled more consistently. The confusion between 'Roof' and 'Tree' and between the 'Roof' and the 'Road' class is largely gone. The CDF result in Fig. 9(d) (with an optimal weight $\beta = 0.5$) shows more homogeneity in some areas of the image and finer delineated structures in other areas, in comparison to the concatenation result. Please note that, although $\beta = 0.5$, this result does not simply reduce to the SVM decision fusion result, since the kernels of both sources, in the final step of the algorithm, are not necessarily the same. To show this, two zoomed examples are shown in Fig. 10. Fig. 10(b) clearly illustrates that the hyperspectral only result is completely lacking clear structure. The CAP only result in Fig. 10(c), on the other hand, is very noisy. Finally, the CDF thematic maps in Fig. 10(e) show much better balancing between the hyperspectral and the contextual features than the concatenation result in Fig. 10(d). Indeed, the

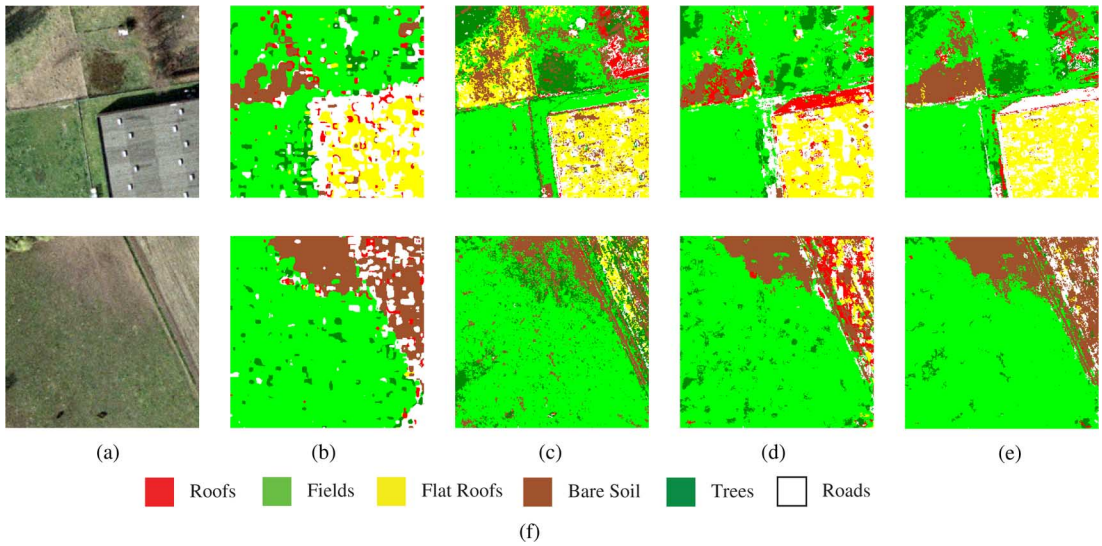

Fig. 10. Zoomed examples for illustrating the effect of combining hyperspectral data and CAP by simple concatenation and CDF on the classification result of the Kalmthout data, (a) True color image. (b) Hyperspectral only. (c) CAP only. (d) Hyperspectral + CAP. (e) CDF. (f) Legend.

transitions between the classes are very sharp and are obviously based on the contextual features. The labels of the pixels in the more homogeneous areas are, on the other hand, primarily based on the spectral features.

V. Conclusion

This article demonstrates how classification of multisource data, consisting of contextual features from a high spatial resolution RGB color image and spectral features from a low spatial resolution hyperspectral image, can be approached by a decision fusion framework in order to produce thematic maps at the spatial resolution of the color image. To extract contextual information, color attribute profiles (CAPs) are introduced. Rather than working on the 'R', 'G', and 'B' bands, the image is transformed into CIE-Lab color space. CAPs are generated by constructing grayscale attribute profiles for the 'L' component, while the 'a' and 'b' components retain their original content. The resulting components are subsequently converted back into RGB space, preserving the color information from the original image. The proposed composite decision fusion (CDF) framework combines a state-of-the-art SVM decision fusion strategy with the approach of composite kernels. The first step of CDF includes feature reduction and generation of more comparable feature sets, in the form of rule images from separate SVM classifiers, based on the SVM decision fusion strategy. The second step comprises classification with a composite kernel SVM, offering the flexibility to put more weight on either the contextual or the spectral features. In a classification experiment on both simulated as well as real multisource data, our CAP is shown to outperform other strategies for generating contextual features and the proposed CDF strategy performs well compared to other methods for performing multisource classification.

Acknowledgment

The authors would like to thank Prof. Paolo Gamba of the University of Pavia, Italy, for the University of Pavia data set along with the training and validation sets. The authors would also like to thank the Flemish Institute for Technological Research (VITO) for the acquisition and preprocessing of the AHS data and the Research Institute for Nature and Forest (INBO) for support on the orthophotographic image. The orthophotographic image is property of the Flemish Geographical Information Agency (AGIV) and the Province of Antwerp, Belgium.

References

[1] M. Herold, M. Gardner, and D. Roberts, "Spectral resolution requirements for mapping urban areas," *IEEE Trans. Geosci. Remote Sens.*, vol. 41, no. 9, pp. 1907–1919, Sep. 2003.

[2] D. Landgrebe, *Signal Theory Methods in Multispectral Remote Sensing*. Hoboken, NJ: Wiley, 2003.

[3] A. Laliberte and A. Rango, "Texture and scale in object-based analysis of subdecimeter resolution unmanned aerial vehicle (UAV) imagery," *IEEE Trans. Geosci. Remote Sens.*, vol. 47, no. 3, pp. 761–770, Mar. 2009.

[4] G. Poggi, G. Scarpa, and J. B. Zerubia, "Supervised segmentation of remote sensing images based on a tree-structured MRF model," *IEEE Trans. Geosci. Remote Sens.*, vol. 43, no. 8, pp. 1901–1911, Aug. 2005.

[5] T. Bau, S. Sarkar, and G. Healey, "Hyperspectral region classification using a three-dimensional gabor filterbank," *IEEE Trans. Geosci. Remote Sens.*, vol. 48, no. 9, pp. 3457–3464, Sep. 2010.

[6] M. Pesaresi and J. A. Benediktsson, "A new approach for the morphological segmentation of high-resolution satellite imagery," *IEEE Trans. Geosci. Remote Sens.*, vol. 39, no. 2, pp. 309–320, Feb. 2001.

[7] J. Angulo, "Morphological colour operators in totally ordered lattices based on distances: Application to image filtering, enhancement and analysis," *Comput. Vis. Image Underst.*, vol. 107, no. 1–2, pp. 56–73, July 2007.

[8] G. Louverdis, M. Vardavoulia, I. Andreadis, and P. Tsalides, "A new approach to morphological color image processing," *Pattern Recognit.*, vol. 35, no. 8, pp. 1733–1741, 2002.

[9] A. Hanbury and J. Serra, "Mathematical morphology in the CIELAB space," *Image Anal. Stereol.*, vol. 21, no. 3, pp. 201–206, 2002.

[10] S. Gibson, J. Bangham, and R. Harvey, "Evaluating a colour morphological scale-space," presented at the British Machine Vision Conf. (BMVC), Norwich, U.K., Jul. 2003.

[11] J. Li and Y. Li, "Multivariate mathematical morphology based on principal component analysis: Initial results in building extraction," in *Proc. 20th ISPRS Congress*, Instanbul, Turkey, 2004, vol. 35, no. B7, pp. 1168–1173.

[12] V. De Witte, S. Schulte, and E. Kerre, "New vector ordering in the RedGreenBlue colour model with application to morphological image magnification," *Int. J. Computat. Intell. Syst.*, vol. 1, no. 2, pp. 103–115, May 2008.

[13] V. De Witte, G. Thoonen, and P. Scheunders, "Classification of multisource images using color morphological profiles," presented at the IEEE IGARSS, Vancouver, Canada, Jul. 2011.
[14] M. Dalla Mura, J. Benediktsson, B. Waske, and L. Bruzzone, "Morphological attribute profiles for the analysis of very high resolution images," *IEEE Trans. Geosci. Remote Sens.*, vol. 48, no. 10, pp. 3747–3762, Oct. 2010.
[15] M. Dalla Mura, J. Benediktsson, and L. Bruzzone, "Classification of hyperspectral images with extended attribute profiles and feature extraction techniques," in *Proc. IEEE IGARSS*, Jul. 2010, pp. 76–79.
[16] M. Dalla Mura, J. Benediktsson, B. Waske, and L. Bruzzone, "Extended profiles with morphological attribute filters for the analysis of hyperspectral data," *Int. J. Remote Sens.*, vol. 31, no. 22, pp. 5975–5991, 2010.
[17] M. Dalla Mura, A. Villa, J. Benediktsson, J. Chanussot, and L. Bruzzone, "Classification of hyperspectral images by using extended morphological attribute profiles and independent component analysis," *IEEE Geosci. Remote Sens. Lett.*, vol. 8, no. 3, pp. 542–546, May 2011.
[18] M. Fauvel, J. Benediktsson, J. Chanussot, and J. Sveinsson, "Spectral and spatial classification of hyperspectral data using SVMs and morphological profiles," *IEEE Trans. Geosci. Remote Sens.*, vol. 46, no. 11, pp. 3804–3814, Nov. 2008.
[19] B. Demir and S. Erturk, "Spectral magnitude and spectral derivative feature fusion for improved classification of hyperspectral images," in *Proc. IEEE IGARSS*, July 2008, vol. 3, pp. III-1020–III-1023.
[20] L. Bruzzone and L. Carlin, "A multilevel context-based system for classification of very high spatial resolution images," *IEEE Trans. Geosci. Remote Sens.*, vol. 44, no. 9, pp. 2587–2600, Sep. 2006.
[21] G. Camps-Valls, L. Gomez-Chova, J. Munoz-Mari, J. Vila-Frances, and J. Calpe-Maravilla, "Composite kernels for hyperspectral image classification," *IEEE Geosci. Remote Sens. Lett.*, vol. 3, no. 1, pp. 93–97, 2006.
[22] D. Tuia, G. Camps-Valls, G. Matasci, and M. Kanevski, "Learing relevant image features with multiple-kernel classification," *IEEE Trans. Geosci. Remote Sens.*, vol. 48, no. 10, pp. 3780–3791, 2010.
[23] B. Waske and S. van der Linden, "Classifying multilevel imagery from SAR and optical sensors by decision fusion," *IEEE Trans. Geosci. Remote Sens.*, vol. 46, no. 5, pp. 1457–1466, 2008.
[24] T. Udelhoven, S. van der Linden, B. Waske, and M. Stellmes, "Hypertemporal classification of large areas using decision fusion," *IEEE Geosci. Remote Sens. Lett.*, vol. 6, no. 3, pp. 592–596, 2009.
[25] J. A. Palmason, J. A. Benediktsson, J. R. Sveinsson, and J. Chanussot, "Classification of hyperspectral data from urban areas using morphological preprocessing and independent component analysis," in *Proc. IEEE IGARSS*, Jul. 2005, pp. 176–179.
[26] E. Breen and R. Jones, "Attribute openings, thinnings and granulometries," *Comput. Vis. Image Underst.*, vol. 64, no. 3, pp. 377–389, 1996.
[27] P. Salembier, A. Oliveras, and L. Garrido, "Anti-extensive connected operators for image and sequence processing," *IEEE Trans. Image Process.*, vol. 7, no. 4, pp. 555–570, Apr. 1998.
[28] C. Kotropoulos and I. Pitas, "Multichannel l filters based on marginal data ordering," *IEEE Trans. Signal Process.*, vol. 42, no. 10, pp. 2581–2595, Oct. 1994.
[29] J. Goutsias, H. J. A. M. Heijmans, and K. Sivakumar, "Morphological operators for image sequences," *Comput. Vis. Image Underst.*, vol. 62, pp. 326–346, Nov. 1995.
[30] N. Jacobson, M. Gupta, and J. Cole, "Linear fusion of image sets for display," *IEEE Trans. Geosci. Remote Sens.*, vol. 45, no. 10, pp. 3277–3288, Oct. 2007.
[31] V. De Witte, "Colour Morphology With Application to Image Magnification," Ph.D. dissertation, Univ. Ghent, Gent, Belgium, 2007.
[32] *Colorimetry: Understanding the CIE System*, J. Schanda, Ed. Hoboken, NJ: Wiley, 2007.
[33] P. Ganesan, V. Rajini, and R. Rajkumar, "Segmentation and edge detection of color images using Cielab color space and edge detectors," in *Proc. Int. Conf. Emerging Trends in Robotics and Communication Technologies (INTERACT)*, Dec. 2010, pp. 393–397.
[34] F. Ortiz, "Image Analysis and Recognition, ser. Lecture Notes in Computer Science," in *Gaussian Noise Removal by Color Morphology and Polar Color Models*, A. Campilho and M. Kamel, Eds. Berlin/Heidelberg: Springer, 2006, vol. 4141, pp. 163–172.
[35] C. Huang, L. Davis, and J. Townshend, "An assessment of support vector machines for land cover classification," *Int. J. Remote Sens.*, vol. 23, no. 4, pp. 725–749, 2002.
[36] G. Foody and A. Mathur, "A relative evaluation of multiclass image classification by support vector machines," *IEEE Trans. Geosci. Remote Sens.*, vol. 42, no. 6, pp. 1335–1343, 2004.
[37] M. Fauvel, J. Chanussot, and J. Benediktsson, "Evaluation of kernels for multiclass classification of hyperspectral remote sensing data," in *Proc. IEEE Int. Conf. Acoustics, Speech and Signal Processing (ICASSP)*, May 2006, vol. 2, pp. 813–816.
[38] C. Chang and C. Lin, LIBSVM: A Library for Support Vector Machines. 2001 [Online]. Available: http://www.csie.ntu.edu.tw/~cjlin/libsvm
[39] M. Varewyck and J.-P. Martens, "A practical approach to model selection for support vector machines with a Gaussian kernel," *IEEE Trans. Syst. Man Cybern. B, Cybern.*, vol. 41, no. 2, pp. 330–340, Apr. 2011.
[40] G. Foody, "Thematic map comparison: Evaluating the statistical significance of differences in classification accuracy," *Photogram. Eng. Remote Sens.*, vol. 70, no. 5, pp. 627–633, May 2004.
[41] G. M. Foody, "Status of land cover classification accuracy assessment," *Remote Sens. Environ.*, vol. 80, no. 1, pp. 185–201, 2002.

Guy Thoonen (S'10) received the M.Sc. degree in 2004 from the Department of Electrical Engineering at Eindhoven University of Technology, The Netherlands. Since April 2007, he is pursuing the Ph.D. degree at the Vision Lab, Department of Physics of the University of Antwerp, Belgium.

His current research is in the field of classification of multispectral and hyperspectral images by including contextual information.

Zahid Mahmood (S'10) received the M.Phil. degree in electronics from Quaid-i-Azam University, Islamabad, Pakistan, in 2000, and the M.Sc. degree in electrical engineering from University of Southern California, Los Angeles, in 2004. He is currently pursuing the Ph.D. degree at the University of Antwerp, Belgium.

His research focus is on hyperspectral image analysis and visualization.

Stijn Peeters received the M.Sc. degree from the Department of Physics, University of Antwerp, Belgium, in 2011, after completing his Master thesis at the Vision Lab, which is part of the same department. The subject of his M.Sc. thesis was "Fusion of hyperspectral images with high-resolution color images for classification".

Paul Scheunders (M'98) graduated in physics in 1986 and received the Ph.D. degree in physics, with work in the field of statistical mechanics, in 1990, from the University of Antwerp, Belgium.

In 1991, he became a research associate at the Vision Lab, Department of Physics, University of Antwerp, where he is now a Professor. He has published over 120 papers in international journals and proceedings in the field of image processing and pattern recognition. His research interests include multiresolution and multispectral image processing for remote sensing.